Properties of the ferroelectric visible light absorbing semiconductors: $Sn_2P_2S_6$ and $Sn_2P_2Se_6$

Yuwei Li and David J. Singh*

Department of Physics and Astronomy, University of Missouri, Columbia, Missouri 65211-7010, USA

(Received 26 September 2017; revised manuscript received 10 November 2017; published 5 December 2017)

Ferroelectrics with suitable band gaps have recently attracted attention as candidate solar absorbing materials for photovoltaics. The inversion symmetry breaking may promote the separation of photoexcited carriers and allow voltages higher than the band gap. However, these effects are not fully understood, in part because of a lack of suitable model systems for studying these effects in detail. Here, we report properties of ferroelectric $Sn_2P_2S_6$ and $Sn_2P_2Se_6$ using first principles calculations. Results are given for the electronic structure, carrier pocket shapes, optical absorption, and transport. We find indirect band gaps of 2.20 eV and 1.55 eV, respectively, and favorable band structures for carrier transport, including both holes and electrons. Strong absorption is found above the direct gaps of 2.43 eV and 1.76 eV. Thus these compounds may serve as useful model systems for understanding photovoltaic effects in ferroelectric semiconductors.

DOI: 10.1103/PhysRevMaterials.1.075402

I. INTRODUCTION

In conventional photovoltaic (PV) devices, electron-hole pairs are created by light absorption and separated by the electric field in a depletion region. The voltage is limited by the band gap. Generally, large band gap photovoltaic devices, which can have relatively high voltage, have lower efficiency because of lower visible light absorption. Ferroelectric photovoltaic devices [1] have been reported since 1962. The photovoltaic charge separation mechanism is apparently different from conventional photovoltaics and the voltage can be significantly higher than the band gap [2,3]. For example, in $BiFeO_3$ [4] the origin of photovoltaic effect was discussed in terms of electron-hole separation at ferroelectric domain walls. Thus it is claimed that inversion symmetry breaking in ferroelectric materials associated with the spontaneous polarization produces an asymmetry that promotes the separation of photoexcited carriers and allows voltages higher than the band gap. The implication of these higher voltages, if not compensated by other losses, is that useful devices with properties distinct from conventional p-n junction solar cells may be possible. However, questions remain, for example, whether the voltage can be maintained in a long duration steady state.

We also note that independent of the charge separation mechanism, high defect tolerance is beneficial in solar absorbers. High dielectric constant is one mechanism for obtaining high defect tolerance, favorable for carrier collection, similar to high dielectric constant radiation detection and energy materials, where the high dielectric constant screens traps and reduces carrier scattering [5–7].

Clearly, photovoltaic effects in ferroelectric materials have attracted considerable recent attention both to understand these effects and because of potential applications [2,8–11]. However, this has been impeded by the lack of good well-characterized ordered ferroelectric semiconductor materials having band gaps in the visible or near infrared that could be used in studies to understand ferroelectric PV effects and the performance that can be obtained from them.

Here we report detailed investigation of the electronic, optical, and related properties of two Sn chalcogenide semiconductor ferroelectrics $Sn_2P_2S_6$ and $Sn_2P_2Se_6$ with band gaps in the visible or near infrared range that may be useful in this context. Prior work on $Sn_2P_2S_6$ has focused mainly on ferroelectric properties, photorefraction, possible memory applications, and characterization of the absorption edges in relation to ferroelectricity [12–30]. $Sn_2P_2Se_6$ has been less studied, but again band edges and ferroelectric properties have been characterized [20,31–33]. The ferroelectric ordering temperatures are $Tc = 337$ K and 193 K for the sulfide and selenide, respectively.

$Sn_2P_2S_6$ and $Sn_2P_2Se_6$ are known ferroelectric materials. Also, they are stoichiometric compounds, as distinct from alloys or superlattice structures. This removes the difficulty of growing and studying superlattices or complications from alloys, and therefore may facilitate detailed investigation of ferroelectric PV phenomena, as well as comparison of experimental and theoretical results for the materials properties of importance for PV application. They also have sizable polarization. The polarization of $Sn_2P_2Se_6$ from hysteresis loop measurements is $\sim$35 $\mu C/cm^2$ at low temperature [19], which is comparable to $BaTiO_3$ (34 $\mu C/cm^2$, in the low T rhombohedral phase). The ferroelectric ordering phase transition has been characterized as second order and the ordering temperature decreases from its value in the ambient pressure sulfide compound, Se alloying, and also with pressure [19,34,35]. The decrease with Se alloying is potentially significant as it would allow one to make ferroelectric samples with different ordering temperatures to characterize for example the effect of proximity to the phase transition on the PV properties. Importantly, these are ordered compounds that have been made as single crystals, which may facilitate characterization and understanding of the interplay of ferroelectricity and PV properties.

II. STRUCTURES AND METHODS

Here we report calculated electronic structures, transport, and optical properties. Our first principles calculations were performed using the linearized augmented plane-wave (LAPW) [36] method as implemented in WIEN2K code [37,38].

*singhdj@missouri.edu

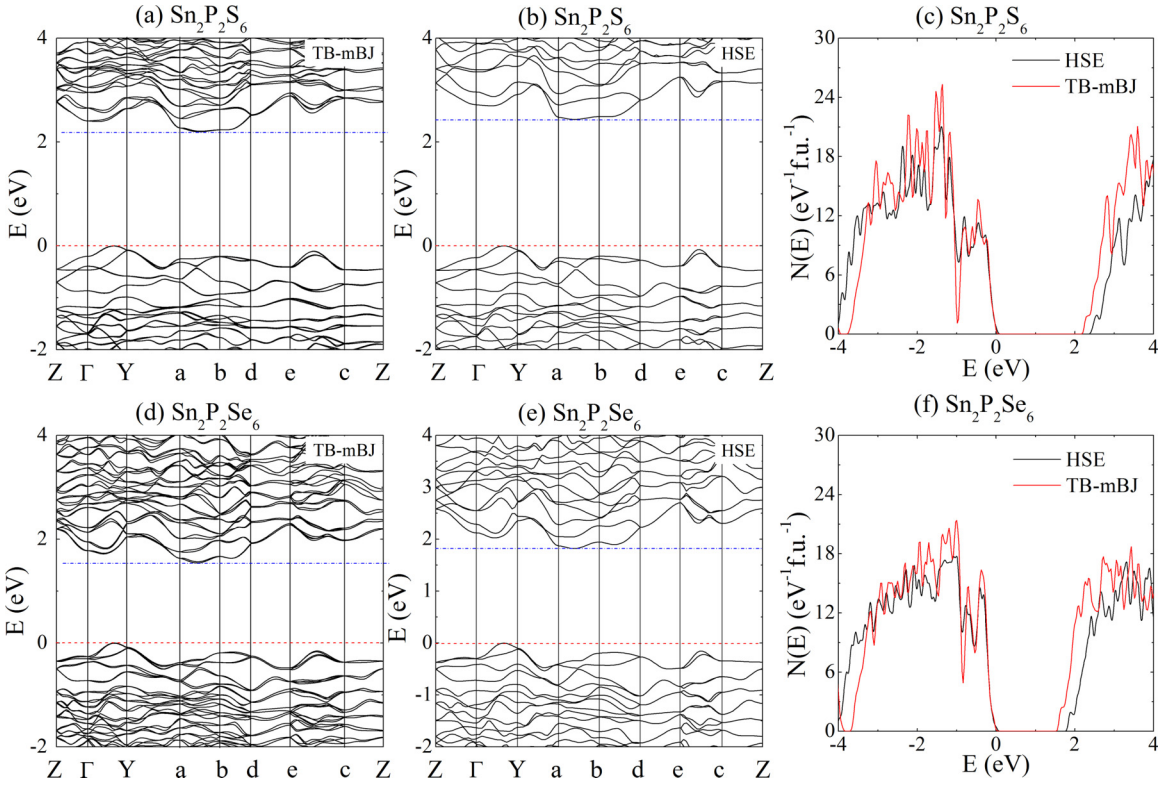

FIG. 1. Calculated band structures [(a),(b),(d),(e)] and densities of states [(c),(f)] for the two compounds comparing TB-mBJ and HSE results. Note that the TB-mBJ results include spin orbit, although as seen the spin-orbit splittings are small. See text for computational details. In all cases, energy zero is at the valence band maximum.

We used LAPW sphere radii of 2.50 Bohr, 1.85 Bohr, and 1.95 Bohr for Sn, P, and S in $Sn_2P_2S_6$ and 2.50 Bohr, 1.86 Bohr, and 2.28 Bohr for Sn, P, and Se in $Sn_2P_2S_6$, respectively. A basis set cutoff, k_{max}, set by the criterion $R_{min}k_{max} = 9.0$ was used, where R_{min} is the P sphere radius. The experimental lattice parameters are $a = 6.529$ Å, $b = 7.485$ Å, $c = 11.317$ Å, and $\beta = 124.11^\circ$ for Pc-$Sn_2P_2S_6$ [15], and $a = 6.815$ Å, $b = 7.717$ Å, $c = 11.694$ Å, and $\beta = 124.549^\circ$ for Pc-$Sn_2P_2Se_6$ [39]. Note that these are pseudo-orthorhombic structures since **a** and **a** + **c** are very nearly orthogonal (angle of $\sim 89^\circ$ in both compounds).

We fixed the lattice parameters to experimental values and relaxed the internal atomic coordinates using the Perdew, Burke, and Ernzerhof generalized gradient approximation (PBE-GGA). This resulting structure is polar as in experiment. Following the structure optimization, we did electronic structure and optical calculations using the modified Becke-Johnson type potential of Tran and Blaha, denoted TB-mBJ in the following [40]. This potential gives band gaps in remarkably good accord with experiment for a wide variety of simple semiconductors and insulators [40–44]. However, it should be noted that the TB-mBJ functional has been shown to disagree with many body calculations for band widths in several cases [45]. We did calculations to cross check TB-mBJ results using the VASP code with the hybrid HSE06 functional [46,47]. A comparison of TB-mBJ and HSE band structures and densities of states is given in Fig. 1. As shown, we find very good agreement in the present case. The most significant differences are in the conduction bands, where the density of states is slightly broader near the band edge for the HSE calculation. One may also note a difference in the valence band width, although this is less significant for the present study since the shape within ~2 eV of the band edge is very much the same.

Spin-orbit coupling (SOC) was included in all TB-mBJ electronic structures and optical property calculations that follow, although the effects are small as may be seen from the small spin orbit splittings in the TB-mBJ band structures (note that the HSE results do not include spin orbit). Transport coefficients were obtained using the BoltzTrap code [48].

III. ELECTRONIC STRUCTURES AND OPTICAL ABSORPTION

We begin with the electronic structures of $Sn_2P_2S_6$ and $Sn_2P_2Se_6$. Figure 1 shows the band structures, and the Brillouin zones with high symmetry points and the carrier pockets are shown in Fig. 2. Both compounds are indirect gap materials.

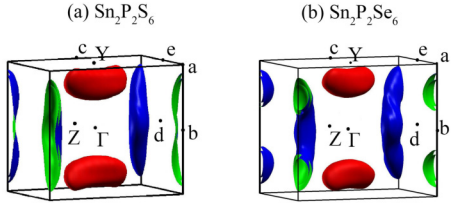

FIG. 2. Calculated isoenergy surfaces illustrating the carrier pockets for $Sn_2P_2S_6$ (a) and $Sn_2P_2Se_6$ (b). Blue/green is used for the n-type isosurface 0.05 eV above CBM and red is used for the p-type isosurface 0.05 eV below VBM.

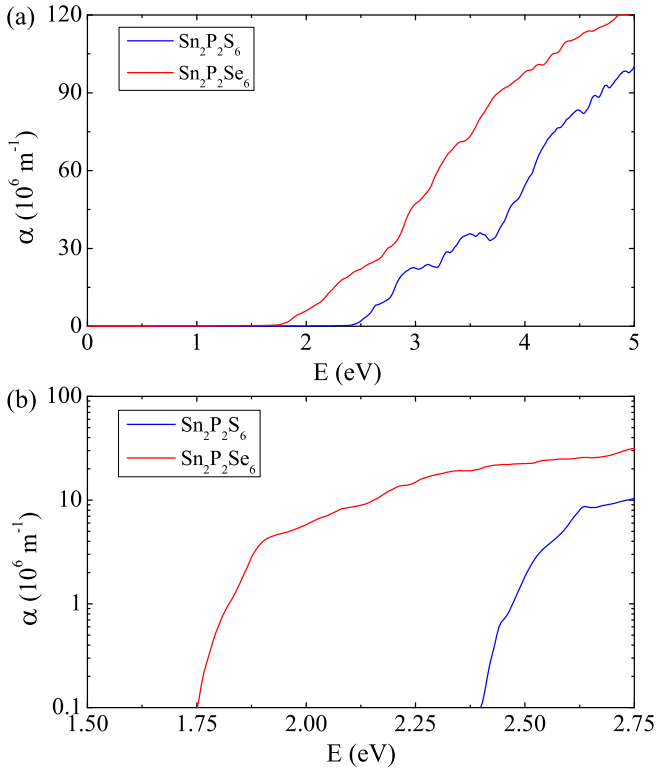

FIG. 3. Calculated absorption coefficient for $Sn_2P_2S_6$ (blue) and $Sn_2P_2Se_6$ (red) with normal scale between 0 and 5 eV (a) and with log scale between 1.5 and 2.75 eV (b). We use very low broadening to make the features more apparent. These are 0.02 eV and 0.005 eV, for (a) and (b), respectively. Note in particular the features near 2.6 eV, 3 eV, and 3.5 eV for the sulfide.

The band gaps of $Sn_2P_2S_6$ and $Sn_2P_2Se_6$ are 2.20 eV and 1.55 eV, respectively. The valence band maxima (VBM) are between Γ and Y points and the conduction band minima (CBM) are between a and b points. The direct band gaps of $Sn_2P_2S_6$ and $Sn_2P_2Se_6$ are 2.43 eV and 1.76 eV, respectively. We find strong optical absorption in $Sn_2P_2S_6$ for short wavelength visible light ($\sim\lambda < 560$ nm) and in $Sn_2P_2Se_6$ for the visible range, as seen in Figs. 3(a) and 3(b). This starts at the absorption edges of 2.40 eV and 1.75 eV, for the sulfide and selenide, respectively.

It is to be noted that in general direct gap semiconductors are preferred in PV applications as the voltage is limited by the fundamental indirect gap. However, photons with energies above the indirect gap but below the direct gap are typically lost due to insufficient absorption leading to reduced efficiency (Si PV cells are an exception). In the present context, the difference between the direct and indirect gaps is not large, and therefore in an actual PV application only a small loss in efficiency due to the indirect gap would be expected, and this might be compensated by reduced electron-hole recombination, also as a result of the indirect nature of the gap.

As mentioned, there have been a number of experimental studies of the absorption at the band edges of these compounds. We compare the experimental band gaps at low temperature with our calculated results in Table I. Reasonable agreement is found. Turning to the region above the band edge, Gamernyk and co-workers [17] reported photoconductivity and photoluminescence spectra for $Sn_2P_2S_6$ crystals up to 3.5 eV. Both spectra show structures at ∼2.7 eV, ∼3.0 eV, and ∼3.4 eV. Our absorption spectrum for $Sn_2P_2S_6$ also shows three main features between the onset and 4 eV. These are a peak at 2.6 eV, a broader peak (with substructure) at ∼3 eV, and another broad peak, again with substructure at ∼3.5 eV, in close correspondence with the features in the experimental spectra.

TABLE I. Direct/indirect gaps compared with low-temperature experimental data.

	$Sn_2P_2S_6$		$Sn_2P_2Se_6$	
	Direct gap (eV)	Indirect gap (eV)	Direct gap (eV)	Indirect gap (eV)
Our work	2.43	2.20	1.76	1.55
A. Ruediger [21]	2.50			
Z. Potůček [23]	2.50			
E. Gerzanich [49]	≈2.65		≈2.00	
J. Lipavičius [32]			≈2.10	

The projected densities of states (pDOS), shown in Fig. 4, indicate the VBM of $Sn_2P_2S_6$ and $Sn_2P_2Se_6$ are mainly dominated by S-3p and Se-4p orbitals, respectively. Especially, there are separate energy ranges for Sn-5s/S-3p and Sn-5s/Se-4p coupling between −7 eV and −6 eV and between −1 eV and 0 eV. This shows divalent Sn as expected [50,51]. It also shows Sn-5s/S-3p (and Sn-5s/Se-4p) bonding states between −7 eV and −6 eV and Sn-5s/S-3p (and Sn-5s/Se-4p) antibonding states between −1 eV and 0 eV.

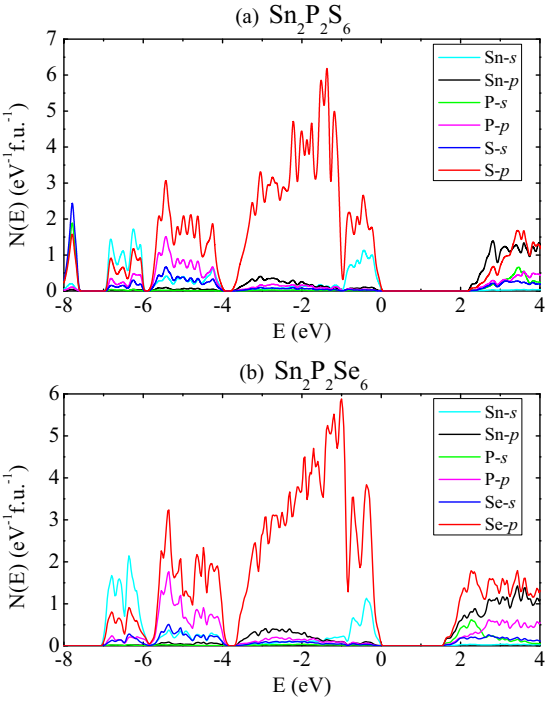

FIG. 4. Projected density of states of $Sn_2P_2S_6$ (a) and $Sn_2P_2Se_6$ (b). The VBM is at zero.

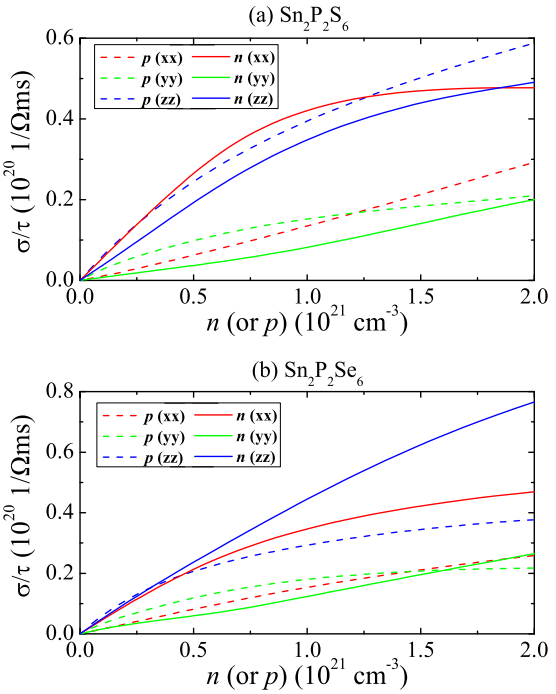

FIG. 5. Calculated anisotropic σ/τ of $Sn_2P_2Se_6$ (a) and $Sn_2P_2Se_6$ (b) as a function of carrier concentration n (or p) at 300 K in xx (red), yy (green), and zz (blue) directions. Solid lines mean n type and dashed lines mean p type.

Antibonding character at a VBM usually causes defect tolerant behavior [52,53], i.e., bond breaking associated with the formation of defect states will produce shallow rather than deep acceptor levels in the midgap region. This greatly facilitates p-type doping, giving rise to ambipolar conductivity in photovoltaic materials, such as chalcopyrites [54]. Previous research indicates the feasibly of p-type conductivity for $Sn_2P_2S_6$ [55] and considering the present results it also seems likely for $Sn_2P_2Se_6$ with suitable dopants or metal vacancies.

IV. TRANSPORT RELATED PROPERTIES

The calculated anisotropic transport function, σ/τ, of $Sn_2P_2S_6$ and $Sn_2P_2Se_6$ at 300 K is shown in Fig. 5. Significantly anisotropic n-type and p-type transport is found. For n-type $Sn_2P_2S_6$, σ/τ in x and z directions are similar and both are larger than that in the y direction (the Cartesian directions are x along **a**, y along **b**, and z normal to the x and y directions, very close to the pseudo-orthorhombic lattice direction $\mathbf{a}+\mathbf{c}$). The p-type σ/τ of $Sn_2P_2S_6$ in the z direction is large, even better than n-type σ/τ for some carrier concentrations. For $Sn_2P_2Se_6$, the n-type and p-type σ/τ in all directions are similar, except the n-type σ/τ in the z direction which is larger than that in other directions. So the electron σ/τ is larger than the hole σ/τ for $Sn_2P_2S_6$. The c-axis direction has the most favorable transport with high σ/τ for both electrons and holes. The effective masses of them have the same anisotropic characteristics with transport properties as seen in Table II. The relatively low m_e^* and m_h^* suggest reasonable carrier transport.

n/p-type $Sn_2P_2S_6$ and $Sn_2P_2Se_6$ have remarkably good σ/τ for materials with complex crystal structures. As can be seen from the parabolic band expression $\sigma/\tau \propto n/m^*$, the origin of the good σ/τ for $Sn_2P_2S_6$ and $Sn_2P_2Se_6$ can be understood in terms of the detailed band structure. For p-type $Sn_2P_2S_6$ and $Sn_2P_2Se_6$, the VBM is derived from two bands, which come from the antibonding coupling of S (or Se) p orbitals with Sn s orbitals. The antibonding coupling increases the upper valence band dispersion, as seen in Fig. 1, decreases the density of states, as seen in Fig. 4, and leads to complex shaped isoenergy surfaces at relatively low carrier concentrations as depicted in Fig. 2. For n type the CBM also comes from dispersive bands and shows complex shaped isosurfaces even at relatively low carrier concentrations that consist of elongated sections (pipes) running along zone edges. These are very far from spherical carrier pockets. This type of isosurface structure, consisting of cylinders or curved cylinders, is also present in cubic p-type PbTe [56] and n-type $SrTiO_3$ [57], which are also materials that show remarkably good conductivity and are near ferroelectricity. As discussed for those materials, this leads to the combination of a relatively light transport effective mass (for conductivity) and heavy density of states effective mass. In the present case light mass dominated by the dispersion transverse to the cylinders enters the conductivity and a heavier mass given by an average enters the density of states [57–62]. The bottom conduction band is highly dispersive across the cylinder directions, contributing strongly to the conductivity, and weakly dispersive along the cylinders, contributing to a high density of states, and thus joint density of states favoring strong absorption.

TABLE II. Direction average and components of the electron (m_e^*) and hole (m_h^*) transport effective mass, obtained from the calculated σ/τ at carrier concentration 10^{18} cm^{-3}.

		Average	xx	yy	zz
$Sn_2P_2S_6$	m_e^*	0.82	0.50	3.61	0.74
	m_h^*	0.81	2.86	0.96	0.43
$Sn_2P_2Se_6$	m_e^*	0.71	0.59	1.53	0.54
	m_h^*	0.69	1.83	0.73	0.41

V. DISCUSSION AND CONCLUSIONS

In summary, we report the electronic structures, transport, and optical properties of ferroelectric $Sn_2P_2S_6$ and $Sn_2P_2Se_6$ based on first principles calculations. They have large visible light absorption and band structures, as seen in the carrier pocket shapes and transport effective masses, consistent with relatively good transport properties. Therefore these compounds are useful model systems for investigating the interplay of ferroelectricity, photoresponse, and charge collection. Besides use for fundamental investigation of PV effects in ferroelectrics, it would also be of interest to investigate them as potential practical solar absorbers. This is because of the reasonable band gap, especially for the selenide. While the selenide is not ferroelectric at room temperature, the high dielectric constant associated with nearness to ferroelectricity and the favorable electronic structure may lead to high defect tolerance and favorable carrier collection. In this regard we note that alloys of the sulfide and selenide have been reported

in which Curie temperature can be tuned to room temperature [35]. Investigation of this alloy may then be useful for studying changes in charge collection as one passes through a ferroelectric transition near room temperature. In any case, the present results suggest investigation of crystalline $Sn_2P_2S_6$ and $Sn_2P_2Se_6$ in order to develop understanding of ferroelectric PV effects in semiconductors.

ACKNOWLEDGMENTS

This work was partly supported by the Department of Energy through the MAGICS center, Award DE-SC0014607 (Y.L., first principles). D.J.S. acknowledges support from the Department of Energy, S3TEC EFRC, Award DE-SC0001299/DE-FG02-09ER46577 (optical properties).

[1] F. Jona and G. Shirane, *Ferroelectric Crystals*, Vol. 1 (Pergamon, New York, 1962).

[2] S. Yang, J. Seidel, S. Byrnes, P. Shafer, C.-H. Yang, M. Rossell, P. Yu, Y.-H. Chu, J. Scott, J. Ager *et al.*, Nat. Nanotechnol. **5**, 143 (2010).

[3] I. Grinberg, D. V. West, M. Torres, G. Gou, D. M. Stein, L. Wu, G. Chen, E. M. Gallo, A. R. Akbashev, P. K. Davies *et al.*, Nature (London) **503**, 509 (2013).

[4] J. Seidel, D. Fu, S.-Y. Yang, E. Alarcón-Lladó, J. Wu, R. Ramesh, and J. W. Ager III, Phys. Rev. Lett. **107**, 126805 (2011).

[5] M.-H. Du and D. J. Singh, Phys. Rev. B **81**, 144114 (2010).

[6] J. Sun and D. J. Singh, Phys. Rev. Appl. **7**, 024015 (2017).

[7] J. Shuai, J. Mao, S. Song, Q. Zhu, J. Sun, Y. Wang, R. He, J. Zhou, G. Chen, D. J. Singh, and Z. Ren, Energy Environ. Sci. **10**, 799 (2017).

[8] V. S. Puli, D. K. Pradhan, R. K. Katiyar, I. Coondoo, N. Panwar, P. Misra, D. B. Chrisey, J. F. Scott, and R. S. Katiyar, J. Phys. D: Appl. Phys. **47**, 075502 (2014).

[9] D. Cao, C. Wang, F. Zheng, W. Dong, L. Fang, and M. Shen, Nano Lett. **12**, 2803 (2012).

[10] M. Qin, K. Yao, and Y. C. Liang, Appl. Phys. Lett. **93**, 122904 (2008).

[11] A. M. Glass, D. Von der Linde, and T. J. Negran, Appl. Phys. Lett. **25**, 233 (1974).

[12] K. Kuepper, B. Schneider, V. Caciuc, M. Neumann, A. V. Postnikov, A. Ruediger, A. A. Grabar, and Y. M. Vysochanskii, Phys. Rev. B **67**, 115101 (2003).

[13] V. V. Shchennikov, N. V. Morozova, I. Tyagur, Y. Tyagur, and S. V. Ovsyannikov, Appl. Phys. Lett. **99**, 212104 (2011).

[14] J. Grigas, E. Talik, V. Lazauskas, Y. M. Vysochanskii, R. Yevych, M. Adamiec, and V. Nelkinas, Ferroelectrics **378**, 70 (2009).

[15] C. Carpentier and R. Nitsche, Mater. Res. Bull. **9**, 1097 (1974).

[16] Y. Tyagur, Ferroelectrics **345**, 91 (2006).

[17] R. Gamernyk, Y. P. Gnatenko, P. Bukivskij, P. Skubenko, and V. Y. Slivka, J. Phys.: Condens. Matter **18**, 5323 (2006).

[18] Z. Potůaček and Z. Bryknar, Ferroelectrics **334**, 171 (2006).

[19] I. P. Studenyak, V. V. Mitrovcij, G. S. Kovacs, O. A. Mykajlo, M. I. Gurzan, and Y. M. Vysochanskii, Ferroelectrics **254**, 295 (2001).

[20] A. Slivka, Ukr. J. Phys. Opt. **2**, 171 (2001).

[21] A. Ruediger, O. Schirmer, S. Odoulov, A. Shumelyuk, and A. Grabar, Opt. Mater. **18**, 123 (2001).

[22] Y. Kojima, A. Okamoto, A. A. Grabar, M. Takabayashi, and K. Shimayabu, Ferroelectrics **378**, 121 (2009).

[23] Z. Potůček, Z. Bryknar, and P. Ptáček, Ferroelectrics **304**, 181 (2004).

[24] A. Shumelyuk and S. Odoulov, J. Opt. **12**, 104015 (2010).

[25] E. Arnautova, E. Sviridov, E. Rogach, E. Savchenko, and A. Grekov, Integr. Ferroelectr. **1**, 147 (1992).

[26] A. Shumelyuk, A. Volkov, S. Odoulov, A. Grabar, I. Stoyka, and D. Evans, Opt. Express **22**, 24763 (2014).

[27] A. Grabar, P. Mathey, and G. Gadret, J. Opt. Soc. Am. B **31**, 980 (2014).

[28] P. Mathey, G. Gadret, A. Grabar, I. Stoika, and Y. Vysochanskii, Opt. Commun. **300**, 90 (2013).

[29] A. Volkov, A. Shumelyuk, S. Odoulov, and M. Imlau, J. Opt. Soc. Am. B **30**, 1102 (2013).

[30] A. Shumelyuk, S. Odoulov, D. Kip, and E. Krätzig, Appl. Phys. B: Lasers Opt. **72**, 707 (2001).

[31] R. Caracas and X. Gonze, Phys. Rev. B **66**, 104106 (2002).

[32] J. Lipavičius, E. Čijauskas, and A. Audzijonis, Phys. Status Solidi B **148**, K97 (1988).

[33] I. Dmitruk, B. Padlyak, O. Grabar, Y. Vysochanskii, and R. Vlokh, Ukr. J. Phys. Opt. **8**, 228 (2007).

[34] S. V. Ovsyannikov, H. Gou, N. V. Morozova, I. Tyagur, Y. Tyagur, and V. V. Shchennikov, J. Appl. Phys. **113**, 013511 (2013).

[35] B. Zapeka, M. Kostyrko, I. Martynyuk-Lototska, and R. Vlokh, Philos. Mag. **95**, 382 (2015).

[36] D. J. Singh and L. Nordstrom, *Planewaves Pseudopotentials and the LAPW Method, 2nd Edition* (Springer, Berlin, 2006).

[37] P. Blaha, K. Schwarz, G. Madsen, D. Kvasnicka, and J. Luitz, WIEN2K, An augmented plane wave + local orbitals program for calculating crystal properties (2001).

[38] K. Schwarz, J. Solid State Chem. **176**, 319 (2003).

[39] R. Israël, R. de Gelder, J. M. M. Smits, P. T. Beurskens, S. W. H. Eijt, Th. Rasing, H. van Kempen, M. M. Maior, and S. F. Motrija, Z. Kristallogr. **213**, 34 (1998).

[40] F. Tran and P. Blaha, Phys. Rev. Lett. **102**, 226401 (2009).

[41] D. Koller, F. Tran, and P. Blaha, Phys. Rev. B **83**, 195134 (2011).

[42] D. J. Singh, Phys. Rev. B **82**, 155145 (2010).

[43] Y.-S. Kim, M. Marsman, G. Kresse, F. Tran, and P. Blaha, Phys. Rev. B **82**, 205212 (2010).

[44] D. J. Singh, Phys. Rev. B **82**, 205102 (2010).

[45] D. Waroquiers, A. Lherbier, A. Miglio, M. Stankovski, S. Ponce, M. J. T. Oliveira, M. Giantomassi, G. M. Rignanese, and X. Gonze, Phys. Rev. B **87**, 075121 (2013).

[46] J. Heyd, G. E. Scuseria, and M. Ernzerhof, J. Chem. Phys. **118**, 8207 (2003).

[47] J. Heyd, G. E. Scuseria, and M. Ernzerhof, J. Chem. Phys. **124**, 219906 (2006).

[48] G. K. H. Madsen and D. J. Singh, Comput. Phys. Commun. **175**, 67 (2006).

[49] E. Gerzanich, Ukr. J. Phys. Opt. **9**, 129 (2008).

[50] A. Walsh and G. W. Watson, Phys. Rev. B **70**, 235114 (2004).

[51] Y. Li, D. J. Singh, M.-H. Du, Q. Xu, L. Zhang, W. Zheng, and Y. Ma, J. Mater. Chem. C **4**, 4592 (2016).

[52] S. B. Zhang, S. H. Wei, A. Zunger, and H. Katayama-Yoshida, Phys. Rev. B **57**, 9642 (1998).
[53] R. E. Brandt, V. Stevanović, D. S. Ginley, and T. Buonassisi, MRS Commun. **5**, 265 (2015).
[54] R. Herberholz, V. Nadenau, U. Rühle, C. Köble, H. Schock, and B. Dimmler, Sol. Energy Mater. Sol. Cells **49**, 227 (1997).
[55] E. M. Golden, S. A. Basun, D. R. Evans, A. A. Grabar, I. M. Stoika, N. C. Giles, and L. E. Halliburton, J. Appl. Phys. **120**, 133101 (2016).
[56] D. J. Singh, Phys. Rev. B **81**, 195217 (2010).
[57] J. Sun and D. J. Singh, APL Mater. **4**, 104803 (2016).
[58] D. Parker, X. Chen, and D. J. Singh, Phys. Rev. Lett. **110**, 146601 (2013).
[59] K. Shirai and K. Yamanaka, J. Appl. Phys. **113**, 053705 (2013).
[60] D. I. Bilc, G. Hautier, D. Waroquiers, G. M. Rignanese, and P. Ghosez, Phys. Rev. Lett. **114**, 136601 (2015).
[61] H. Shi, D. Parker, M. H. Du, and D. J. Singh, Phys. Rev. Appl. **3**, 014004 (2015).
[62] G. Xing, J. Sun, Y. Li, X. Fan, W. Zheng, and D. J. Singh, Phys. Rev. Materials **1**, 065405 (2017).